The Loss of an Electrostatic Contact Unique to AMPA Receptor Ligand Binding Domain 2 Slows Channel Activation

ARTICLE *in* BIOCHEMISTRY · APRIL 2012

Impact Factor: 3.02 · DOI: 10.1021/bi3001837 · Source: PubMed

7 AUTHORS, INCLUDING:

Sandra M. Holley
University of California, Los Angeles
10 PUBLICATIONS **88** CITATIONS
SEE PROFILE

Gregory A Weiland
Cornell University
40 PUBLICATIONS **1,827** CITATIONS
SEE PROFILE

Linda M Nowak
Cornell University
42 PUBLICATIONS **5,133** CITATIONS
SEE PROFILE

Published in final edited form as:
Biochemistry. 2012 May 15; 51(19): 4015–4027. doi:10.1021/bi3001837.

Loss of an Electrostatic Contact Unique to AMPA Receptor Ligand-Binding Domain 2 Slows Channel Activation[†]

Sandra M. Holley[§,¶], **Ahmed H. Ahmed**[§], **Jayasri Srinivasan**[§], **Swetha E. Murthy**[¥], **Gregory A. Weiland**[§], **Robert E. Oswald**[§], and **Linda M. Nowak**[§,*]

[§]Department of Molecular Medicine, Cornell University, Ithaca, NY 14853 USA

[¥]Department of Biochemistry, University at Buffalo, Buffalo, NY 14214 USA

Abstract

Ligand-gated ion channels undergo conformational changes that transfer the energy of agonist binding to channel opening. Within ionotropic glutamate receptor (iGluR) subunits, this process is initiated in their bilobate ligand binding domain (LBD) where agonist binding to lobe 1 favors closure of lobe 2 around the agonist and allows formation of interlobe hydrogen bonds. AMPA receptors (GluAs) differ from other iGluRs because glutamate binding causes an aspartate-serine peptide bond in a flexible part of lobe 2 to rotate 180° (flipped conformation), allowing these residues to form cross-cleft H-bonds with tyrosine and glycine in lobe 1. This aspartate also contacts the sidechain of a lysine residue in the hydrophobic core of lobe 2 by a salt bridge. We investigated how the peptide-flip and electrostatic contact (D655-K660) in GluA3 contribute to receptor function by examining pharmacological and structural properties with an antagonist (CNQX), a partial agonist (kainate) and two full agonists (glutamate and quisqualate) in wildtype and two mutant receptors. Alanine substitution decreased agonist potency of $GluA3_i$-D655A and $GluA3_i$-K660A receptor-channels expressed in HEK293 cells and differentially affected agonist binding affinity to isolated LBDs without changing CNQX affinity. Correlations observed in the crystal structures of the mutant LBDs included loss of the D655-K660 electrostatic contact, agonist-dependent differences in lobe1/lobe2 closure and unflipped D(A)655-S656 bonds. Glutamate-stimulated activation was slower for both mutants, suggesting that efficient energy transfer of agonist binding within the LBD of AMPA receptors requires an intact tether between the flexible peptide flip domain and the rigid hydrophobic core of lobe 2.

Glutamate mediates excitatory synaptic transmission in brain by activation of AMPA (GluA1–4), kainate (GluK1–5) and NMDA (GluN1–3) receptors. The molecular diversity of the ionotropic glutamate receptor (iGluR) subfamilies is important for their divergent functional roles. AMPA receptors mediate fast synaptic transmission in the central nervous system, while NMDA channels, with slower activation, high Ca^{2+} permeability, and voltage-sensitivity to block by external and internal Mg^{2+} ions, act as coincidence detectors

[†]This work was supported by a grant from the National Institutes of Health (R01 NS049223). It includes research conducted at the Cornell High Energy Synchrotron Source (CHESS), which is supported by the National Science Foundation under award DMR-0936384, using the Macromolecular Diffraction at CHESS (MacCHESS) facility, which is supported by award GM103485 from the National Institutes of Health, through its National Institute of General Medical Sciences.

[*]Corresponding Author: Linda M. Nowak, Department of Molecular Medicine, C3-117 Veterinary Medical Center, Cornell University, Ithaca, NY 14853, phone: (607) 253-3655, lmn1@cornell.edu.
[¶]Present address: Department of Psychiatry and Biobehavioral Sciences, UCLA, Los Angeles, CA 90024.

Supporting Information Available: Figures S1 and S3 provide examples of raw data traces from whole cell recordings used to generate the graphs in Figures 2 and 4 respectively. Figure S2 shows the crystal structure of the GluA3 LBD with the antagonists CNQX in the binding site. Figure S4 shows the decrease in intrinsic fluorescence as the wildtype and mutated LBD proteins were heated. This material is available free of charge via the Internet at http://pubs.acs.org.

at the synapse (1) and activate transduction mechanisms for nuclear signaling (2–4). Together, AMPA and NMDA receptors mediate activity-dependent synaptic plasticity underlying learning and memory formation (5–8), and Ca^{2+}-permeable AMPA channels contribute to excitotoxic cell death in epilepsy, hypoxic ischemia and neurodegenerative diseases (8–11). Deeper understanding of AMPA receptor activation will be useful for developing agents to regulate sleep and respiration, and to treat some forms of epilepsy and cognitive disorders whose pathological features are related to dysregulation of GluA receptor function.

Knowledge of the conformational changes and molecular rearrangements that contribute to agonist activation of GluA receptors is essential to understanding how drugs might be designed to modify channel function. Detailed structures of the ligand binding domains of iGluRs (12–15) showed that ligands bind in a cleft between the two lobes in the LBD (Figure 1A, GluA3 with quisqualate bound). AMPA receptor LBDs bound to full agonists are closed by 20–22° relative to unliganded apo structures, and there is a 180° rotation around a peptide bond in lobe 2 hypothesized to play a role in receptor activation (12, 16). In this flipped position, there is an additional hydrogen bond between the carbonyl of D655 through a water molecule to the amide of Y452 and another between the carbonyl of S656 and the amide of G453 (Figure 1B). D655 also forms a salt bridge with K660 of GluA3 (Figure 1C). This salt bridge is seen GluA structures, and as suggested by primary sequences and observed in crystal structures of other iGluR LBDs (Figure 1D), it appears to be unique to AMPA-type iGluR receptors (14, 15, 17, 18).

The activation of ligand-gated receptors has been described as a wave of conformational changes starting with the initial interaction of agonist with the receptor and ending in the opening of the channel gate (19, 20). We hypothesized that the D655–K660 salt bridge may contribute to the transmission of the energy of agonist binding to channel opening by tethering D655 to the F-helix in the hydrophobic core of lobe 2 and investigated this by single alanine substitutions at each residue. Comparing wildtype and mutant LBD structures demonstrated the loss of the D655–K660 salt bridge and changes in binding affinity that were ligand-dependent. Electrophysiological analysis revealed increased agonist EC_{50} values (decreased potency), and glutamate response activation was slower for both mutations. Together these observations provide evidence that the energy of agonist induced conformational changes in the LBD is transmitted more effectively to the channel when the D655–K660 salt bridge is intact, and further support a role for the peptide flip conformational change in AMPA receptor activation.

Materials and Methods

Plasmids, mutations and cells

Plasmids for rat wildtype GluA3-*flip* ($GluA3_i$) and two mutant subunits were constructed in the laboratory. Rat wildtype GluA3-*flop* cDNA ($GluA3_o$) (gift of Stephen Heinemann, Salk Institute, San Diego, CA) was excised from pBluescript and transferred to the pRK5 (Stratagene, LaJolla, CA) mammalian expression vector. The flop sequence was replaced by a flip sequence containing the cyclothiazide (CTZ) binding site and a glycine (G747) residue at the R/G editing site obtained by PCR amplification using GluA3 specific primers in an E14 mouse brain cDNA library (gift of James Eberwine, Univ. Pennsylvania, Philadelphia, PA). The blasticidin® resistance gene was excised from pE/BSD (Invitrogen, Carlsbad, CA) and transferred to the pRK5/r-$mGluA3_i$ construct into the Hpa I site distal to the SV40 polyadenylation sequence. The aspartate to alanine mutation (D655A) was made in the pRK5/r-$mGluA3_i$ plasmid using the QuikChange® (Stratagene) mutagenesis kit. The pRK5/r-$mGluA3_i$/Bsd, pE/r-$mGluA3_i$-D655A/Neo and pE/r-$mGluA3_i$-K660A/Neo transfection

plasmids were completely sequenced in overlapping reactions performed in both directions (Cornell University BioResource Center, Ithaca, NY).

Three sets of cell lines stably expressing wildtype $GluA3_i$, $GluA3_i$-D655A or $GluA3_i$-K660A receptors in human embryonic kidney (HEK293) cells lacking the T antigen (ATCC, Manassas, VA) were used in the majority of experiments. Cells were co-transfected with a puromycin expression vector pUR (Clontech, Mountain View, CA) and one of the $GluA3_i$ plasmids in a 1:3 ratio using cationic lipid-based transfection reagents (PolyFect®, QIAGEN, Valencia, CA; or Lipofectamine™ 2000, Invitrogen). Eighteen to 24 hrs later, cells were exposed to 10 μg/ml puromycin (Sigma-Aldrich, St. Louis, MO) for 1–2 hrs and then washed with FBS-containing DMEM. Surviving cells were challenged with selection antibiotics (20–25 μg/ml blasticidin (Invitrogen) or 1.5–2.5 mg/ml geneticin (G418) to establish stable cell lines. Single colonies of cells were isolated and expanded under continuous antibiotic selection. Cell lines expressing 0.3 to 1 nA glutamate-evoked current per cell in whole cell recordings were frozen (DMEM with 20% FBS and 8.5% DMSO) at −80°C and used later in recordings. These cells and HEK293T cells (ATCC, Manassas, VA; 21) were transiently transfected to boost receptor expression for the fast glutamate application experiments in outside-out patches with the appropriate receptor cDNA plus the pE/BFP plasmid (Clontech) using the PolyFect® reagent (QIAGEN) in a 3:1 plasmid ratio (1.8 μg cDNA/35 mm dish). All cells were cultured and maintained in Dulbeco's modified MEM (Gibco/Invitrogen) supplemented with 10% fetal bovine serum (FBS; Gemini Bioproducts, West Sacramento, CA).

Electrophysiology

Whole cell patch clamp recordings were performed at room temperature (22–24°C) as described by Hamill et al. (22) using an EPC7 amplifier (HEKA Instruments Inc., Bellmore, NY). Recordings were performed 24–72 hrs after passage or 24–48 hrs after transfection, using pipettes (3–4 MΩ, TW150, WPI, Sarasota, FL,) filled with (in mM): 120 CsCl, 10 EGTA/Ca^{2+} and 10 HEPES/KOH (pH 7.35). The external bath solution contained (in mM): 150 NaCl, 2.8 KCl, 1.0 $CaCl_2$, 10 HEPES/NaOH (pH 7.4). Data were digitized at a rate 2.5- to 5-times the total filter cut-off frequency and analyzed using laboratory software or with QuB software (www.qub.buffalo.edu).

Agonists in this study included: (+)-α-amino-3-hydroxy-5-methylisoxazole-4-proprioniate (S-AMPA; Tocris Bioscience, Ellisville, MO), L-glutamate (Sigma-Aldrich, St. Louis, MO), L-quisqualate, (Ascent Scientific LLC, Princeton, NJ, or Tocris Bioscience), kainate (Tocris Bioscience or Ascent Scientific). The non-NMDA antagonist used was 6-cyano-7-nitroquinoxaline-2,3-dione (CNQX; Tocris Bioscience or Ascent Scientific). Stock solutions (10 to 100 mM) of GluA receptor agonists and CNQX were prepared in deionized distilled water with equimolar amounts of NaOH and the pH was adjusted to 7.2–7.4. Cyclothiazide (CTZ; Tocris Bioscience or Ascent Scientific) was prepared as a 50 mM stock solution in absolute methanol. All recording solutions contained 100–150 μM CTZ.

Agonist concentration-effect data were obtained for wildtype and mutant $GluA3_i$ receptors by applying them over a range of concentrations and normalizing their responses in each cell to the 10 mM glutamate response. Cell stability was usually assessed by repeating applications of 100 μM glutamate or 300 μM kainate during the recording. Drugs were applied at room temperature (20–22°C) by slow bath perfusion through a Warner Instruments (Hamden, CT) MP-8 manifold to cells voltage-clamped at −60 mV. Concentration-effect data shown in Figure 2 were fit (Origin 7; OriginLab Corp., Northampton, MA) with the Hill equation:

$$I = I_{agonist_{\max}} \left(\frac{[agonist]^{n_H}}{[agonist]^{n_H} + (EC_{50})^{n_H}} \right)$$

where I is the agonist-evoked current at [*agonist*], $Iagonist_{\max}$ is the peak current at the saturating concentration of agonist, [*agonist*] is the concentration of the agonist, EC_{50} is the concentration of the agonist that elicits a half-maximal response, and n_H is the Hill coefficient.

Schild analysis (23) was performed to compare the binding affinity of the wildtype and D655A receptors for the competitive antagonist CNQX. CNQX was used near its 50% inhibition concentration (IC_{50}), which was determined against a concentration of agonist that did not fully saturate the receptor. The dose-ratio (DR) values (Figure 4A) were determined from the shift in the agonist response curves produced in the presence of three different concentrations of CNQX that bracketed the IC_{50} values for wildtype and $GluA3_i$-D655A mutant receptors.

Outside-out macropatch recordings were used to determine on- and off-response time constants. Pipettes (1.5–3.0 MΩ) were filled with (in mM): 135 CsF, 33 CsOH, 2 $MgCl_2$, 1 $CaCl_2$, 10 HEPES and 11 EGTA, adjusted to pH 7.4 (CsOH). Cells and excised patches were bathed in (extracellular) solutions containing (in mM): 150 NaCl, 2.5 KCl, 1.0 $CaCl_2$, 10 HEPES pH 7.4. Lightly pressurized (0.02 to 0.06 mPa) extracellular solutions (control or glutamate) were applied through a glass theta tube (2.0 mm diameter; Harvard Apparatus, Holliston, MA), which produced two streams with a sharp interface between them (24). Theta tubes were treated with concentrated hydrofluoric acid for 20–25 min to decrease the septum thickness. Each barrel of the theta tube was connected to three solutions through a micro-manifold controlled with pinch valves (VC6; Warner Instruments). The recording pipette containing the excised patch was positioned within a stream of control solution close to the interface. The theta tube was moved to from position one to two so the second stream (containing one of two different glutamate solutions with 100–200 μM CTZ) was applied to the patch and returned to position one using a piezoelectric mechanical translator (Burleigh LSS-3100/3200) allowing for measurement of the on- and off- response time constants. Currents were low-pass filtered at 2, 5 or 10 kHz (Axopatch 200B; 4-pole Bessel), sampled at 10 or 50 kHz (Digidata, 1440A; Molecular Devices, Sunnyvale, CA) using pClamp 10.2 software. Each trial included a 50 ms prepulse of control solution, followed by a 2.5 or 5 s application of glutamate with CTZ, followed by control solution for 14 s. Control solution was applied continuously to the patch while the agonist solution for the next trial was preloaded into the other barrel during the unrecorded 100 s interval between trials. CTZ-containing control solution was applied to the patch for 30 s at the end of the 100 s interval, prior to initiation of the next drug trial. All CTZ-containing solutions were made fresh every 2 h to insure that desensitization did not interfere with the measurements.

Agonist application velocity was deduced by open-tip potential measurements made at the end of each recording using a 50%-dilute control solution in the agonist application barrel. Data were included in Figure 6C if the 10 – 90% exchange occurred within 0.3 ms. Macropatch current traces were analyzed in Clampfit 10.2 and the on and off-responses were fit with a single exponential function:

$$y = y_o + A_1 e^{-x/\tau}$$

where y_o represents the y offset, A_1 the amplitude and τ the time constant (pClamp 10.2). Note that the value of τ is a relaxation (eigenvalue) that does not necessarily correspond to an individual rate constant in a kinetic mechanism. When peak currents were less than −10 pA, 3 to 8 data traces were averaged before fitting.

Radioligand Binding

The soluble LBD domain of wildtype, GluA3-D655A and GluA3-K660A mutations were expressed and purified as described by Chen et al. (25) and by Ahmed et al. (17). Binding to isolated LBD proteins was performed in a buffer containing (in mM): 30 HEPES, 100 KSCN and 2.5 $CaCl_2$ with 10% glycerol, pH 7.2 (with NaOH). All solutions were maintained at 4°C. Glutamate was removed from the LBD proteins by successive concentration and dilution in buffer, and protein was diluted to a final concentration of ~2 nM. After the addition of [^{3}H]AMPA (46 Ci/mmol; PerkinElmer, Waltham, MA) the reaction (200 μl in duplicate) with competing ligands (AMPA, CNQX, glutamate, kainate and quisqualate,) proceeded for 1 hour followed by filtration through GSWP filters (Millipore, Bedford, MA) and two 2 ml washes with binding buffer. Analysis was done using Kaleidagraph (Synergy Software, Reading, PA). Competition for [^{3}H]-AMPA binding with unlabelled AMPA was used to determine changes in AMPA affinity and to convert the IC_{50} values to K_i values according to the Cheng-Prusoff equation (26).

Thermal stability

Intrinsic tryptophan fluorescence measured with a Varian Cary Eclipse spectrofluorimeter (excitation wavelength of 280 nm; emission wavelength of 336 nm) was used to measure thermal unfolding. The temperature was monitored continuously and changed at a rate of 0.06°C/min from 10 and 70°C. For the measurements, protein was diluted to 1–2 μM in 10 mM glutamate, 25 mM sodium acetate pH 6.0, 25 mM sodium chloride, and 1 mM sodium azide. Data were analyzed using Kaleidagraph (Synergy Software) as described by Madden *et al.* (27).

Structural Analysis

For crystallization trials, the proteins were concentrated to 0.2 to 0.5 mM using a Millipore Centricon 10 centrifugal filter. Ligands were exchanged into the sample by successive concentration (Amicon Ultra-4 (10K) filter) and dilution using buffer in the first eight steps followed by four washes in the presence of ligand. The final protein concentration was approximately 0.3 mM. The final ligand concentrations were 10 mM for L-glutamate, 5 mM for kainate and CNQX, and 2 mM for quisqualate. All crystals were grown at 4°C using the hanging drop technique, and the drops contained a 1:1 (*v/v*) ratio of protein solution to reservoir solution. In all cases, the reservoir solution was 15–16% polyethylene glycol (PEG) 8K, 0.05–0.1 M sodium cacodylate, 0.25 M ammonium sulfate, and 0.1 M zinc acetate (pH 6.5). Both flip ($GluA3_i$) and flop ($GluA3_o$) variants were tested and those providing crystals with satisfactory refraction are reported.

Data were collected at the Cornell High Energy Synchrotron Source beam line A1 using a Quantum-210 Area Detector Systems charge-coupled device detector. Data sets were indexed and scaled with HKL-3000 (28). Structures were solved with molecular replacement using Phenix (29). Refinement was performed with Phenix (29) and Coot 0.7 (30) was used for model building. Domain orientation was determined as described by Gill *et al* (18). Orientations are reported as closures or openings relative to the structure of $GluA3_i$ bound to glutamate reported previously (3dln, 17).

Results

Functional effects of loss of the Asp-Lys salt bridge

The pharmacological profile of wildtype $GluA3_i$ receptor-channels was compared to those of $GluA3_i$-D655A and $GluA3_i$-K660A mutant receptors expressed in HEK293 cells in the presence of 100–150 μM CTZ, which suppresses desensitization of flip splice variant GluA receptors (31) and slows deactivation (32). Agonist-dependent functional differences between the wildtype and mutants are illustrated in Figure 2 and supplemental data (Figure S1). Cells exposed to glutamate (10 mM) and quisqualate (5 mM) gave similar maximum current responses while kainate (5 mM) was a partial agonist. Concentration-effect curves fitted with the Hill equation showed that the Hill slope increased in both D655A and K660A mutants for glutamate from 1.3 (wildtype) to 1.5 (D655A), to 2.0 (K660A). EC_{50} values for all three agonists were increased in the mutants relative to wildtype (Figure 2A, B, D), but the magnitude of the EC_{50} shifts differed among the agonists (Table 1). The D655A mutation had its greatest effect on glutamate's EC_{50} and its least effect on kainate's while the K660A mutation was the opposite. Kainate's efficacy was increased relative to glutamate in the D655A mutant ($p < 0.05$; 36 ± 2% in the wildtype, $n = 9$; compared to 48 ± 6%, $n = 6$ for the D655A mutant). This difference in kainate efficacy did not appear to be due to a change in steady-state desensitization since kainate responses from cells expressing wildtype and $GluA3_i$-D655A receptor-channels were potentiated to the same extent by 30, 100 and 300 μM CTZ (Figure S1).

Binding affinity is decreased for agonists but not for the antagonist CNQX

We investigated the binding affinity of the agonists used in the EC_{50} studies in the isolated LBD for wildtype and mutant receptors because an increase in EC_{50} in a holo receptor can arise from a decrease in the intrinsic binding affinity for ligands, or from changes subsequent to binding due to conformational changes reflecting receptor activation and/or deactivation kinetics. Competition binding assays for several ligands were performed in purified preparations of wildtype, GluA3-D655A and GluA3-K660A LBD proteins using [^{3}H]AMPA to determine IC_{50} values (Figure 3, Table 1). Both mutations decreased AMPA affinity by ~2-fold (K_i values increased), and glutamate and quisqualate affinity also decreased in the D655A (7.6- and 8.4-fold respectively) and K660A mutants (2.5- and 6-fold respectively) compared to wildtype. The binding results for kainate followed a different pattern (Figure 3C). While the K_i for kainate was essentially unchanged in the D655A mutant relative to wildtype, it increased by nearly 10-fold in the K660A mutant, which is consistent with the larger shift in kainate's EC_{50} in the K660A mutant. While the affinity of full agonists decreased significantly, competition against [^{3}H]AMPA using the antagonist CNQX produced nearly identical curves for wildtype and both mutants (Figure 3D), and the K_i values for CNQX were similar in wildtype and in the D655A and K660A mutant LBDs.

Table 1 summarizes pharmacological parameters including EC_{50}, IC_{50} and K_i values and for wildtype and the mutant GluA3 receptors (Figure 2, 3). Function-to-binding ratios (EC_{50} or K_b to K_i) were calculated to facilitate comparisons between the different assays (42). In the wildtype GluA3, the ratio was <10 for CNQX, 15 for kainate, ~1200 for glutamate and 5000 for quisqualate (Figure 4A). There is a large difference between agonist potency (EC_{50}) and binding affinity (K_i) for full agonists, while for the partial agonist kainate, where the activation of the channel is less probable, the EC_{50} to K_i ratio was much smaller. For the competitive antagonist CNQX we compared the K_b obtained from Schild analysis (see below) to K_I ratio and found the the ratio was less than 10. In the mutant receptors, the increase in K_i was greater than the change in EC_{50} for glutamate and quisqualate in the D655A mutant (Figure 4B). For kainate, K_i was not significantly changed in the D655A mutant, but the EC_{50} increased, which increased the potency to affinity ratio by 3-fold. In

the K660A mutant, the K_i and EC_{50} values increased a comparable amount for kainate, maintaining the relationship between potency and binding affinity.

CNQX action and affinity unchanged by D655A mutation

Previous studies reported that some mutations in GluA receptors convert CNQX to a partial agonist (33). The mechanism of inhibition and the affinity for an antagonist can be determined in a functional assay without kinetic modeling using Schild analysis (34–37) using an antagonist that occupies the same binding site as agonists and makes many of the same contacts. In GluA2 LBD, CNQX was shown to occupy the same site as agonists (38). To verify that this was also the case for GluA3, we determined the structure of GluA3i bound to CNQX (1.8 Å, Figure S2 and Table S1), and found that the structure was very similar to that determined for GluA2 (lobe opening relative to $GluA3_i$ bound to glutamate for GluA2-CNQX was 13.8 ± 0.04° and for $GluA3_i$-CNQX was 13.3 ± 0.6°). Neither wildtype nor $GluA3_i$-D655A receptor-channels responded to direct application of 0.2–20 μM CNQX (data not shown). It was a fully reversible inhibitor of glutamate-evoked responses in wildtype and $GluA3_i$-D655A receptor-channels so it was used to obtain concentration-inhibition curves against 200 μM glutamate in wildtype $GluA3_i$ and 1600 μM glutamate in $GluA3_i$-D655A receptors. IC_{50} values for CNQX were 1.5 ± 0.3 μM and 1.2 ± 0.3 μM for wildtype and mutant respectively. These parameters were used to design the protocol for the Schild analysis (supplemental data Figure S3). Partial glutamate concentration-effect curves were obtained in the presence of 0.2, 1.0 and 2.0 μM CNQX for wildtype and $GluA3_i$-D655A Figure 5A shows the slopes of these curves were unchanged in CNQX. Dose-ratio (DR) values, calculated from the shifts in the glutamate concentration-effect curves for the wildtype and D655A mutant receptors (Figure 5A), were plotted against the CNQX concentration in Figure 5B (Schild plot). The log-linear slopes were 0.88 and 0.86 for the wildtype and D655A mutant respectively, indicating that CNQX is a competitive antagonist in the mutant and wildtype receptors. By convention, the data were re-fitted with a fixed slope of 1.0 to obtain the affinity for CNQX (K_b), which was 0.96 μM in the wildtype and 1.0 μM in the $GluA3_i$-D655A mutant receptors. Thus, functional analysis indicated that CNQX affinity was unchanged by the D655A mutation.

It is noteworthy that ratio of the CNQX K_b determined in the *holo* receptors, and the K_i determined in the isolated LBDs was <10, indicating that functional affinity and binding affinity are very similar. In contrast, full agonists have very large EC_{50}:K_i ratios, which were decreased in the mutants, but remained at least two orders of magnitude larger than the K_b/K_i ratio for CNQX. The high ratios observed for the full agonists most likely stem from the block of desensitization by cyclothiazide for EC_{50} measurements, while the K_i measured in LBD binding assays is the thermodynamic equivalent of an agonist-induced desensitized receptor conformation. This interpretation is also consistent with the kainate data, since this partial agonist does not completely desensitize wildtype or $GluA3_i$-D655A receptor-channels (Figure S1 D–E), and it has an EC_{50} to K_i ratio closer to CNQX than to the full agonists (<50 *vs* >1000 for glutamate; Table 1).

Glutamate response activation is slower in both mutants

In the isolated LBD, the binding affinity of CNQX for either the D655A or the K660A mutation was unchanged compared to wildtype, as was the affinity determined by Schild analysis measuring responses in the $GluA3_i$-D655A mutant receptor-channels. This suggests that at least the initial step of ligand binding, the docking of the ligand in lobe 1, is not affected by these mutations.

We investigated the effects of the D655A and K660A mutations on response kinetics by rapidly applying glutamate to excised membrane patches (Figure 6A, B) using a

piezoelectric mechanical translation device (24). Despite measures to increase receptor expression (see methods), outside-out macropatches contained few channels and typically responses were small, particularly for the $GluA3_i$-D655A mutant.

When 1 mM and 5 mM glutamate were applied to patches containing wildtype or the D655A mutant, response amplitude increased as predicted by whole cell concentration-effect data (Figure 2) and response rise-time decreased. Time constant values for response onset (τ_{on}) in patches expressing wildtype $GluA3_i$ decreased from 5.5 ± 0.6 ms (n = 4) to 1.7 ± 0.2 ms (n = 4) to 0.8 ± 0.1 ms (n = 5) as glutamate concentration increased from 1 to 5 to 10 mM (Figure 6C). τ_{on} was significantly longer for patches expressing $GluA3_i$-D655A mutant channels exposed to 1 mM (9.7 ± 0.8 ms, n = 5; p = 0.01) and 5 mM glutamate (6.9 ± 0.7 ms n = 4; p = 0.02) than in wildtype. Responses of patches expressing $GluA3_i$-K660A receptors to 10 mM glutamate (τ_{on} = 3.2 ± 0.5 ms; n = 5) were significantly slower (p < 0.01) than observed for wildtype $GluA3_i$ (0.8 ± 0.1 ms; n = 5).

The time constant for channel closing (τ_{off}) was measured for 5 and/or 10 mM glutamate in wildtype (τ_{off} = 3.4 ± 0.6 ms), $GluA3_i$-D655A (τ_{off} = 3.4 ± 0.3 ms) and $GluA3_i$-K669A (τ_{off} = 4.1 ± 1.0 ms). Comparing the wildtype and mutant responses, onset was faster for wildtype than for the mutants, and channel closing (deactivation) was unaffected. These results are consistent with a slowing of the activation rate, which includes the steps of ligand binding to lobe 1, which evidence from the CNQX data suggests is unaffected, and agonist-induced receptor activation (lobe closure, Asp-Ser peptide flip, interlobe H-bond formation, and channel opening), for $GluA3_i$-receptor-channels when the D655-K660 salt bridge is lost.

Thermal stability of D655A and K660A mutations decreases relative to wildtype LBDs

The thermal unfolding of the wildtype, D655A, and K660A GluA3i LBDs bound to glutamate was measured with intrinsic tryptophan fluorescence. The increase in temperature from 10° to 70°C resulted in a linear decrease in fluorescence overlayed with a transition associated with protein unfolding (Figure S4). Both mutants were less stable than wildtype, with T_m values of 49.1°C, 52.6°C, and 57.1°C for D655A, K660A, and wildtype, respectively.

Crystal structures of the wildtype and D655A mutant LBDs

Crystals structures of glutamate-, quisqualate-, and kainate-bound wildtype and GluA3-D655A mutant LBDs and the kainate-bound K660A mutant were determined to investigate whether these mutations altered the protein structure bound to the different agonists. Despite repeated attempts, crystals obtained for the K660A mutant bound to quisqualate and glutamate did not refract sufficiently well to obtain a structure. The structures of the binding sites are presented in Figures 7 and 8 and structural statistics are in Table S1.

Wildtype structures—The structures of wildtype $GluA3_i$ (3dln, 17; 1.91 Å) and $GluA3_o$ (3m3k, 39; 1.79 Å) LBD bound to glutamate were reported previously. $GluA3_i$ LBD had one structure in the asymmetric unit with a flipped peptide bond (Figure 7A, C). $GluA3_o$ had three structures in the asymmetric unit and the peptide bond was flipped in all three cases. Relative to $GluA3_i$, the lobe orientation of the three structures of $GluA3_o$ was 1.9 ± 0.6° more closed. The structure of $GluA3_i$ bound to quisqualate was determined to 1.7 Å, with one structure in the asymmetric unit. A second structure was also determined to 1.75 Å, but it was essentially identical to the first, so that only one is described in Table S1. In both cases, the D655/S656 peptide bond was flipped (Figure 7D, F). The structures had lobe orientations essentially the same as $GluA3_i$ bound to glutamate. Two wildtype structures of $GluA3_i$ LBD bound to kainate were determined to 1.8 and 2.2 Å resolution (Figure 8A, D; Table S1). The lobe1/lobe2 cleft closure of wildtype $GluA3_i$ bound to kainate (6.1 ± 0.45°)

was similar to the GluA4 kainate-bound structure (5.8°; 18) and greater than in GluA2 (8.8°; 13). At least part of the reason for this is that the terminal methyls of L654 are rotated by 180° in both GluA3 and GluA4, allowing the lobes to move closer together. Gill et al. (18) also attributed the closer approach of the two lobes to phenylalanine in position 703 in GluA4 (F706 in GluA3) *versus* tyrosine in GluA2. The loss of the hydroxyl in GluA4 results in a loss of one of two waters that form a H-bond network to kainate. As in GluA2 and GluA4, the D6556/S656 peptide bond is not flipped in any GluA3 structures bound to kainate (Figure 8).

D655A-Glutamate—We obtained structures of the D655A mutant $GluA3_o$ LBD bound to glutamate for four separate crystals (1.8–1.9 Å; Table S1). The structures did not differ significantly, so that only one is reported in Table S1. In all cases, the A655/S656 peptide bond was unflipped (Figure 7B, C). The lobes were open by 2.8 ± 0.2° relative to the wildtype $GluA3_i$. The effect of the D655A mutation seems to be two-fold. First, the salt bridge with K660 is lost, and secondly, the tendency to form H-bonds across the lobe interface may be decreased. The decrease in the propensity to form the H-bonds is likely due to the fact that the backbone carbonyl of the residue at position 655 can also rotate to interact with the side chain of K660. In this orientation, the peptide bond is not flipped and the H-bonds cannot form in the D655A mutation, thus stabilizing the unflipped conformation of the peptide bond upon removing the salt bridge.

D655A-Quisqualate—For the D655A mutant, two structures were obtained for $GluA3_o$ LBD bound to quisqualate from different crystals (1.8 and 2.2 Å), but there was only one copy in each (Figure 7E, F; Table S1). In both cases, the peptide backbone for A655/S656 appeared to be flipped, but the density was weaker than the remainder of the protein (Figure 7F, right). In one structure, the hydrogen-bonding pattern (A655-H_2O-Y452; S656-G453) was clearly present; however, the A655-H_2O-Y452 H-bond was not observed in the other structure. In both cases, a flipped structure seemed to be most consistent with the data; but lower contours of the density map suggested that both flipped and unflipped conformations were likely present. Lobe orientation was the same for both the wildtype and D655A mutant bound to quisqualate, and did not differ from wildtype $GluA3_i$ bound to glutamate.

D655A-Kainate—Two unique structures of kainate bound to D655A mutant $GluA3_o$ LBD were found in the asymmetric unit (2.25 Å; Figure 8B, D). Like the wildtype, the A655/S656 bond was unflipped. The lobes of the two structures were open by 5.5 and 3.6 Å relative to wildtype $GluA3_i$ bound to glutamate. One of the two structures was more closed than the wildtype structure, in part due to a further rotation of the L654 sidechain.

K660A-Kainate—The GluA3-K660A LBD structure bound to kainate (Figure 8C) was refined to 2.1 Å (Table S1). The L654 sidechain was in the same orientation as wildtype (Figure 8C) and lobe1/lobe2 closure was similar to wildtype bound to kainate (open by 5.6° relative to $GluA_i$ bound to glutamate). The sidechain of D655 in the K660A mutant is rotated almost 180° around the beta carbon to point toward the cleft (Figure 8D). This may allow it to interact with the positively charged sidechain of K688. The kainate-bound K660A mutation also shows a change in the E661-R664 salt bridge. The sidechain of R664 moves in the direction of the lobe interface and occupies space that was vacated when K660 was replaced by alanine, and E661 moves away from the lobe1/2 interface. This also positions the sidechain of R664 to interact with the carbonyl of D655 (Figure 8D). These changes may be responsible for the small twist of lobe 2 in the K660A mutant observed with kainate bound, which very likely stabilizes the unflipped conformation. These changes are consistent with the increase in kainate EC_{50} observed for this mutant.

Discussion

$GluA3_i$ homomeric receptor-channels expressed in HEK293 cells share features of the AMPA receptors expressed in the early stages of brain development (40), including fast opening- and closing-rates (41) and high permeability to Ca^{2+} (42). Defining the mechanism of activation of GluA receptors is critically important to understanding their regulation in health and disease. Sobolevsky et al. (43) provided a detailed structural analysis of the full GluA2 receptor-channel (minus the C-terminus) which showed that both the amino terminal domains and LBDs form pairs of dimers. Linkers between the LBD and the M1 and M3 transmembrane helices connect the binding domain to the four-fold symmetrical ion channel and participate in channel gating. Our study is focused on lobe 2 of the GluA LBD where the 180° rotation of a peptide bond between an Asp residue and the adjacent serine (D655 and S656 in GluA3) is proposed to play a role in AMPA receptor activation (12, 16). In GluA receptors, this Asp also makes an electrostatic contact with a Lys residue located in the helix F of lobe 2 (D655 and K660 in GluA3), thus linking the flexible peptide flip domain to the hydrophobic core of lobe 2. Through a series of pharmacological and structural studies using the isolated GluA3 LBD and the *holo* receptor-channel, we observed a relationship between agonist-dependent structural differences in receptors with mutations in the LBD and functional changes in the *holo* receptor. Our findings suggest the electrostatic interaction between the peptide flip Asp residue and Lys 660 may favor the rotation of the D655/S656 peptide bond and formation of two cross-cleft H-bonds that may allow a more efficient transfer of the energy of agonist-induced conformational changes to channel opening.

Neither the D655A nor the K660A mutation changed the binding affinity of the antagonist CNQX, and Schild analysis showed no change in the affinity of CNQX in $GluA3_i$-D655A receptors relative to wildtype, indicating these mutations are unlikely to affect the docking of the ligand with lobe 1. Slower activation of $GluA3_i$-D655A and $GluA3_i$-K660A receptor-channels without a change in response-off kinetics (Figure 6) indicates that one or more of the steps leading to channel opening are affected by the mutations. The increase in the Hill slopes of the glutamate and quisqualate response curves, which was more apparent in $GluA3_i$-K660A receptors, suggests that activation of partially bound tetrameric mutant receptors may be less likely than in wildtype $GluA3_i$. A full interrogation of the differences in channel gating of these mutants will require rigorous systematic single channel analysis, which will be challenging given the complexity of AMPA receptor-channel gating (44–47).

Structural correlates of GluA activation

The activation of ligand-gated receptors involves a series of conformational changes that starts with the initial interaction of agonist with the receptor and ends with the opening of a permeation pathway. At least three conformational changes associated with GluA channel activation occur within the LBD: 1) diffusion of the ligand and docking with lobe 1, 2) closure of the lobes and interaction of the ligand with lobe 2, and 3) formation of H-bonds across the lobe interface, which involves D655 and S656 (16).

CNQX functioned as a competitive antagonist (Figure 5). Crystal structures with CNQX show it interacts with lobe 1 and to some extent with lobe 2 (Figure S2), but only rarely is lobe closure observed with CNQX bound (48). The effects of the mutations were only minimal on CNQX affinity measured in the radioligand binding assay for both mutants, and in the Schild analysis of the wildtype and D655A *holo* receptors.

Kainate can progress through all three states, but, like CNQX, full closure of the lobes and formation of H-bonds across the interface are relatively rare events (48). The D655A mutation did not affect kainate binding to the LBD and had only a small effect on the EC_{50}.

In contrast, the K660A mutation affected both binding and EC_{50} to a much greater extent, which is most likely due to the changes in the electrostatic interactions of D655 with K688 and R664 (Figure 8C).

Rapid application of glutamate revealed that the response on-rate was slower for the mutants while the off-rate was unchanged. The question is, at what step or steps from ligand docking in lobe 1 through to channel opening do these mutations slow the activation process that occurs with full agonists. Since CNQX affinity and function were not affected, the differences observed for quisqualate and glutamate in these mutants most likely stem from changes during and after closure of the lobes around the agonist and not during the initial binding step. Whole cell recordings showed the effect on glutamate EC_{50} was greater in the D655A mutant than in the K660A mutant, while both $GluA3_i$-D655A and $GluA3_i$-K660A receptor-channel activation was slower for glutamate in the excised patches, indicating the mutations do not produce equivalent effects. Likewise, the thermal stability of $GluA3_i$ bound to glutamate was decreased in both mutants, with D655A less stable than K660A. The structural changes causing decreased glutamate function in the D655A mutant are consistent with a decreased stability of the “flipped” conformation of the D655A-S656 peptide bond in the mutant, which in the wildtype GluA3 LBD would otherwise make interlobe H-bonds. In the flipped conformation, the backbone carbonyl of D655 makes a water-mediated H-bond to the backbone amide of Y452, and the sidechain of D655 interacts with the sidechain of K660 in the wildtype. In the D655A mutant, the sidechain interaction with K660 is eliminated, but the backbone carbonyl of A655 in the unflipped conformation can interact electrostatically with the sidechain of K660. This would also stabilize the unflipped conformation of the backbone relative to the flipped conformation, perhaps further decreasing the propensity to form the H-bond in the mutant. The crystal structures appear to be consistent with this interpretation, since when glutamate was bound the peptide bond was unflipped in the mutant but not in the wildtype. The effect of the D655A mutation on quisqualate EC_{50} was less than that observed with glutamate, and in the crystal structure the peptide bond was flipped with quisqualate bound; however, the electron density for D655 and S656 was decreased, suggesting motion between the two states. The functional changes observed for kainate in the D655A mutant were somewhat different. The EC_{50} shift was smaller, and surprisingly the efficacy of kainate measured relative to that of glutamate and quisqualate was increased. However, this result could also be explained if the efficacy of full agonists had decreased. The kainate bound GluA3-D655A structure showed only a small change in lobe orientation relative to wildtype and the peptide bond was in the unflipped position in both cases. Moreover, the binding affinity for kainate in the isolated LBD was similar for wildtype and the D655A mutant.

The crystal structure for the K660A mutant bound to kainate showed that the loss of the K660 sidechain might also be expected to decrease the stability of the flipped conformation, since the sidechain of D655 is no longer positioned away from the lobe interface by an electrostatic interaction with K660. In fact, in the kainate-bound K660A structure, the backbone carbonyl of D655 interacts with R664 in the unflipped conformation, and the sidechain rotates toward the lobe interface and interacts with K688. There was a greater effect of the K660A mutation on the kainate EC_{50} compared to the other agonists, and it was accompanied by a significant decrease in ligand binding affinity.

Even though the changes in the structures may explain the decrease in binding affinity and the slower channel response caused by these mutations, we cannot rule out the possibility that the slower activation observed in the mutants involves steps beyond the formation of the interlobe H-bonds, and may involve structural rigidity within lobe 2. Maltsev has shown that lobe 2 consists of a β-sheet sandwiched between two hydrophobic cores (49). The connections between the hydrophobic cores and the β-sheet show dynamics on the μs-ms

timescale. Thus, it is conceivable that the electrostatic interaction between K660 (within one hydrophobic core) and D655 is part of a system of electrostatic contacts that stabilizes lobe 2 and efficiently translates the energy of lobe closure to the linkers that connect the LBD to the ion channel domain of the protein. Severing one of these connections could weaken the link and perhaps slow the rate of activation.

Conclusions

We examined AMPA receptor activation with D655A and K660A mutations in a wildtype $GluA3_i$ background. Both mutations slowed glutamate-stimulated activation and produced modest changes in agonist-binding affinity, while showing no effects on antagonist affinity or channel closing kinetics. Changes in the D655A mutant interlobe H-bond network for glutamate, kainate and quisqualate correlated with observed EC_{50} changes, and support the hypothesis that the peptide flip region plays a role in GluA activation. D655A and K660A mutations break an electrostatic contact with K660 in helix F, which tethers the peptide flip domain to helix F in wildtype receptors. Along with helix G, helix F is part of a hydrophobic core that has minimal additional interactions within the central β-sheet of lobe 2 (49). It is possible that the K660/D655 salt bridge is one of several electrostatic interactions that may contribute to rigidity in lobe 2 and permit efficient transduction of agonist binding energy to the ion channel linker.

Supplementary Material

Refer to Web version on PubMed Central for supplementary material.

Acknowledgments

Dr. Stephen Heinemann provided the GluA3-flop cDNA and Dr. James Eberwine provided the E14 mouse brain library and expert advice. Ms. Heather Larkin provided technical assistance. We thank Drs. David Deitcher, Ronald Harris-Warrick, Huai-Hu Chuang and Kinning Poon for helpful discussions.

Abbreviations

AMPA	a-amino-3-hydroxy-5-methyl-4-isoxazole-propionic acid
CNQX	6-cyano-7-nitroquinoxaline-2,3-dione
CTZ	cyclothiazide (6-chloro-3,4-dihydro-3-(5-norbornen-2-yl)-2*H*-1,2,4-benzothiazidiazine-7-sulfonamide-1,1-dioxide)
FW	(*S*)-5-fluorowillardiine ((S)-(−)-α-amino-5-fluoro-3,4-dihydro-2,4-dioxo-1(2H)pyridinepropanoic acid)
GluA1–4	four subtypes of AMPA receptor
$GluA2_o$	flop form of GluA2
$GluA3_i$	flip form of GluA3
GluK1–5	five subtypes of kainate receptor
iGluR	ionotropic glutamate receptor
KA	kainate
LBD	extracellular ligand-binding domain of GluA2 and GluA3
NMDA	N-methyl-D-aspartic acid

References

1. Dingledine R, Borges K, Bowie D, Traynelis S. The glutamate receptor ion channels. Pharmacol Rev. 1999; 51:7–61. [PubMed: 10049997]
2. Lee YS, Silva AJ. The molecular and cellular biology of enhanced cognition. Nat Rev Neurosci. 2009; 10:126–140. [PubMed: 19153576]
3. Cohen S, Greenberg ME. Communication between the synapse and the nucleus in neuronal development, plasticity, and disease. Annu Rev Cell Dev Biol. 2008; 24:183–209. [PubMed: 18616423]
4. Ghosh A, Carnahan J, Greenberg ME. Requirement for BDNF in activity-dependent survival of cortical neurons. Science. 1994; 263:1618–1623. [PubMed: 7907431]
5. Citri A, Malenka RC. Synaptic plasticity: multiple forms, functions, and mechanisms. Neuropsychopharmacology. 2008; 33:18–41. [PubMed: 17728696]
6. Derkach VA, Oh MC, Guire ES, Soderling TR. Regulatory mechanisms of AMPA receptors in synaptic plasticity. Nat Rev Neurosci. 2007; 8:101–113. [PubMed: 17237803]
7. Lau CG, Zukin RS. NMDA receptor trafficking in synaptic plasticity and neuropsychiatric disorders. Nat Rev Neurosci. 2007; 8:413–426. [PubMed: 17514195]
8. Liu SJ, Zukin RS. Ca2+-permeable AMPA receptors in synaptic plasticity and neuronal death. Trends Neurosci. 2007; 30:126–134. [PubMed: 17275103]
9. Heath PR, Shaw PJ. Update on the glutamatergic neurotransmitter system and the role of excitotoxicity in amyotrophic lateral sclerosis. Muscle Nerve. 2002; 26:438–458. [PubMed: 12362409]
10. Hynd MR, Scott HL, Dodd PR. Glutamate-mediated excitotoxicity and neurodegeneration in Alzheimer's disease. Neurochem Int. 2004; 45:583–595. [PubMed: 15234100]
11. Steenland HW, Kim SS, Zhuo M. GluR3 subunit regulates sleep, breathing and seizure generation. Eur J Neurosci. 2008; 27:1166–1173. [PubMed: 18312590]
12. Armstrong N, Gouaux E. Mechanisms for activation and antagonism of an AMPA-sensitive glutamate receptor: crystal structures of the GluR2 ligand binding core. Neuron. 2000; 28:165–181. [PubMed: 11086992]
13. Armstrong N, Sun Y, Chen GQ, Gouaux E. Structure of a glutamate-receptor ligand-binding core in complex with kainate. Nature. 1998; 395:913–917. [PubMed: 9804426]
14. Mayer ML. Crystal structures of the GluR5 and GluR6 ligand binding cores: Molecular mechanisms underlying kainate receptor selectivity. Neuron. 2005; 45:539–552. [PubMed: 15721240]
15. Furukawa H, Gouaux E. Mechanisms of activation, inhibition and specificity: crystal structures of the NMDA receptor NR1 ligand-binding core. EMBO J. 2003; 22:2873–2885. [PubMed: 12805203]
16. Fenwick MK, Oswald RE. On the mechanisms of alpha-amino-3-hydroxy-5-methylisoxazole-4-propionic acid (AMPA) receptor binding to glutamate and kainate. J Biol Chem. 2010; 285:12334–12343. [PubMed: 20110361]
17. Ahmed AH, Wang Q, Sondermann H, Oswald RE. Structure of the S1S2 glutamate binding domain of GluR3. Proteins. 2009; 75:628–637. [PubMed: 19003990]
18. Gill A, Birdsey-Benson A, Jones BL, Henderson LP, Madden DR. Correlating AMPA receptor activation and cleft closure across subunits: crystal structures of the GluR4 ligand-binding domain in complex with full and partial agonists. Biochemistry. 2008; 47:13831–13841. [PubMed: 19102704]
19. Grosman C, Zhou M, Auerbach A. Mapping the conformational wave of acetylcholine receptor channel gating. Nature. 2000; 403:773–776. [PubMed: 10693806]
20. Millhauser GL, Salpeter EE, Oswald RE. Diffusion models of ion-channel gating and the origin of power-law distributions from single-channel recording. Proc Natl Acad Sci U S A. 1988; 85:1503–1507. [PubMed: 2449693]
21. Huang Z, Li G, Pei W, Sosa LA, Niu L. Enhancing protein expression in single HEK 293 cells. J Neurosci Methods. 2005; 142:159–166. [PubMed: 15652630]

22. Hamill OP, Marty E, Neher B, Sakmann B, Sigworth FJ. Improved patch-clamp techniques for high-resolution current recording from cells and cell-free membrane patches. Pflügers Archiv. 1981; 391:85–100.
23. Verdoorn TA, Kleckner NW, Dingledine R. N-methyl-D-aspartate/glycine and quisqualate/kainate receptors expressed in Xenopus oocytes: antagonist pharmacology. Mol Pharmacol. 1989; 35:360–368. [PubMed: 2564633]
24. Amico-Ruvio SA, Murthy SE, Smith TP, Popescu GK. Zinc Effects on NMDA Receptor Gating Kinetics. Biophys J. 2011; 100:1910–1918. [PubMed: 21504727]
25. Chen GQ, Sun Y, Jin R, Gouaux E. Probing the ligand binding domain of the GluR2 receptor by proteolysis and deletion mutagenesis defines domain boundaries and yields a crystallizable construct. Protein Sci. 1998; 7:2623–2630. [PubMed: 9865957]
26. Cheng Y, Prusoff WH. Relationship between the inhibition constant (K_I) and the concentration of inhibitor which causes 50 per cent inhibition (I_{50}) of an enzymatic reaction. Biochem Pharmacol. 1973; 22:3099–3108. [PubMed: 4202581]
27. Madden DR, Abele R, Andersson A, Keinanen K. Large-scale expression and thermodynamic characterization of a glutamate receptor agonist-binding domain. Eur J Biochem. 2000; 267:4281–4289. [PubMed: 10866833]
28. Otwinowski, Z.; Minor, W. Processing of X-ray diffraction data collected in oscillation mode. In: Carter, CW.; Sweet, RM., editors. Methods in Enzymology, Vol. 276, Macromolecular Crystallography, part A. Academic Press; New York: 1997. p. 307-326.
29. Adams PD, Grosse-Kunstleve RW, Hung LW, Ioerger TR, McCoy AJ, Moriarty NW, Read RJ, Sacchettini JC, Sauter NK, Terwilliger TC. PHENIX: building new software for automated crystallographic structure determination. Acta Crystallogr D Biol Crystallogr. 2002; 58:1948–1954. [PubMed: 12393927]
30. Emsley P, Cowtan K. Coot: model-building tools for molecular graphics. Acta Crystallogr D Biol Crystallogr. 2004; 60:2126–2132. [PubMed: 15572765]
31. Partin KM, Patneau DK, Mayer ML. Cyclothiazide differentially modulates desensitization of alpha-amino-3-hydroxy-5-methyl-4-isoxazoepropionic acid receptor splice variants. Molecular Pharmacology. 1994; 46:129–138. [PubMed: 8058047]
32. Mitchell NA, Fleck MW. Targeting AMPA receptor gating processes with allosteric modulators and mutations. Biophys J. 2007; 92:2392–2402. [PubMed: 17208968]
33. Taverna F, Xiong ZG, Brandes L, Roder JC, Salter MW, MacDonald JF. The Lurcher mutation of an alpha-amino-3-hydroxy-5-methyl- 4-isoxazolepropionic acid receptor subunit enhances potency of glutamate and converts an antagonist to an agonist. J Biol Chem. 2000; 275:8475–8479. [PubMed: 10722683]
34. Colquhoun D. Binding, gating, affinity and efficacy: the interpretation of structure-activity relationships for agonists and of the effects of mutating receptors. Br J Pharmacol. 1998; 125:924–947. [PubMed: 9846630]
35. Colquhoun D. What have we learned from single ion channels? J Physiol. 2007; 581:425–427. [PubMed: 17363381]
36. Schild HO. Drug antagonism and pAx. Pharmacol Rev. 1957; 9:242–246. [PubMed: 13465304]
37. Wyllie DJ, Chen PE. Taking the time to study competitive antagonism. Br J Pharmacol. 2007; 150:541–551. [PubMed: 17245371]
38. Menuz K, Stroud RM, Nicoll RA, Hays FA. TARP auxiliary subunits switch AMPA receptor antagonists into partial agonists. Science. 2007; 318:815–817. [PubMed: 17975069]
39. Ahmed AH, Ptak CP, Oswald RE. Molecular Mechanism of Flop Selectivity and Subsite Recognition for an AMPA Receptor Allosteric Modulator: Structures of GluA2 and GluA3 in Complexes with PEPA. Biochemistry. 2010; 49:2843–2850. [PubMed: 20199107]
40. Cull-Candy S, Kelly L, Farrant M. Regulation of Ca2+-permeable AMPA receptors: synaptic plasticity and beyond. Curr Opin Neurobiol. 2006; 16:288–297. [PubMed: 16713244]
41. Pei W, Huang Z, Niu L. GluR3 flip and flop: differences in channel opening kinetics. Biochemistry. 2007; 46:2027–2036. [PubMed: 17256974]
42. Varney MA, Rao SP, Jachec C, Deal C, Hess SD, Daggett LP, Lin F, Johnson EC, Velicelebi G. Pharmacological characterization of the human ionotropic glutamate receptor subtype GluR3

stably expressed in mammalian cells. J Pharmacol Exp Ther. 1998; 285:358–370. [PubMed: 9536032]

43. Sobolevsky AI, Rosconi MP, Gouaux E. X-ray structure, symmetry and mechanism of an AMPA-subtype glutamate receptor. Nature. 2009; 462:745–756. [PubMed: 19946266]
44. Poon K, Ahmed AH, Nowak LM, Oswald RE. Mechanisms of Modal Activation of GluA3 Receptors. Mol Pharmacol. 2011; 80:49–59. [PubMed: 21464198]
45. Poon K, Nowak LM, Oswald RE. Characterizing single-channel behavior of GluA3 receptors. Biophys J. 2010; 99:1437–1446. [PubMed: 20816055]
46. Prieto ML, Wollmuth LP. Gating modes in AMPA receptors. J Neurosci. 2010; 30:4449–4459. [PubMed: 20335481]
47. Zhang W, Cho Y, Lolis E, Howe JR. Structural and single-channel results indicate that the rates of ligand binding domain closing and opening directly impact AMPA receptor gating. J Neurosci. 2008; 28:932–943. [PubMed: 18216201]
48. Ahmed AH, Wang S, Chuang HH, Oswald RE. Mechanism of AMPA receptor activation by partial agonists: disulfide trapping of closed lobe conformations. J Biol Chem. 2011; 286:35257–35266. [PubMed: 21846932]
49. Maltsev AS, Oswald RE. Hydrophobic side chain dynamics of a glutamate receptor ligand binding domain. J Biol Chem. 2010; 285:10154–10162. [PubMed: 20110365]

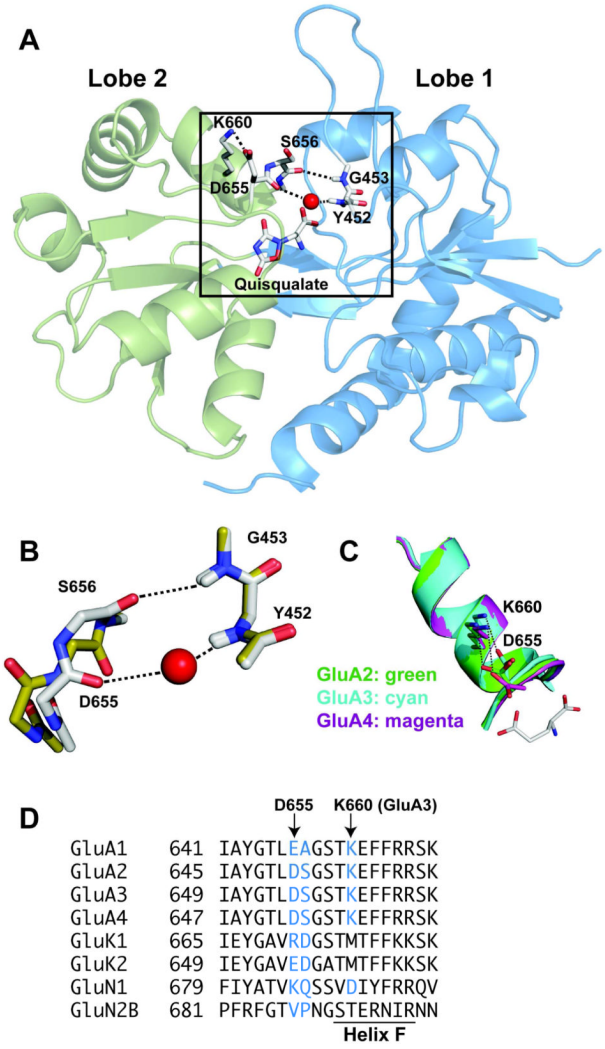

Figure 1. Structural elements of iGluRs

A) The structure of $GluA3_o$ LBD with quisqualate bound. The D655-S656 peptide bond is in the flipped form and the red sphere indicates the position of a water molecule. The ligand-binding site (box) is featured in Figures 7, 8 and S2. B) Flipped (white carbon atoms) and unflipped (yellow carbon atoms) forms of the peptide bond illustrate the H-bonds across the lobe interface for the flipped form, which includes one contact through a water molecule. C) The electrostatic contact between the peptide-flip Asp and the Lys residue in helix F tethers the flexible loop to the hydrophobic core in lobe 2 of GluA receptors. The stick representation of glutamate marks the position of the binding site at the end of the helix. D) Partial sequence alignment of a portion of lobe 2 for a series of AMPA, kainate and NMDA receptors. Arrows indicate positions mutated in this study (D655A and K660A in GluA3); residues in helix F are marked below.

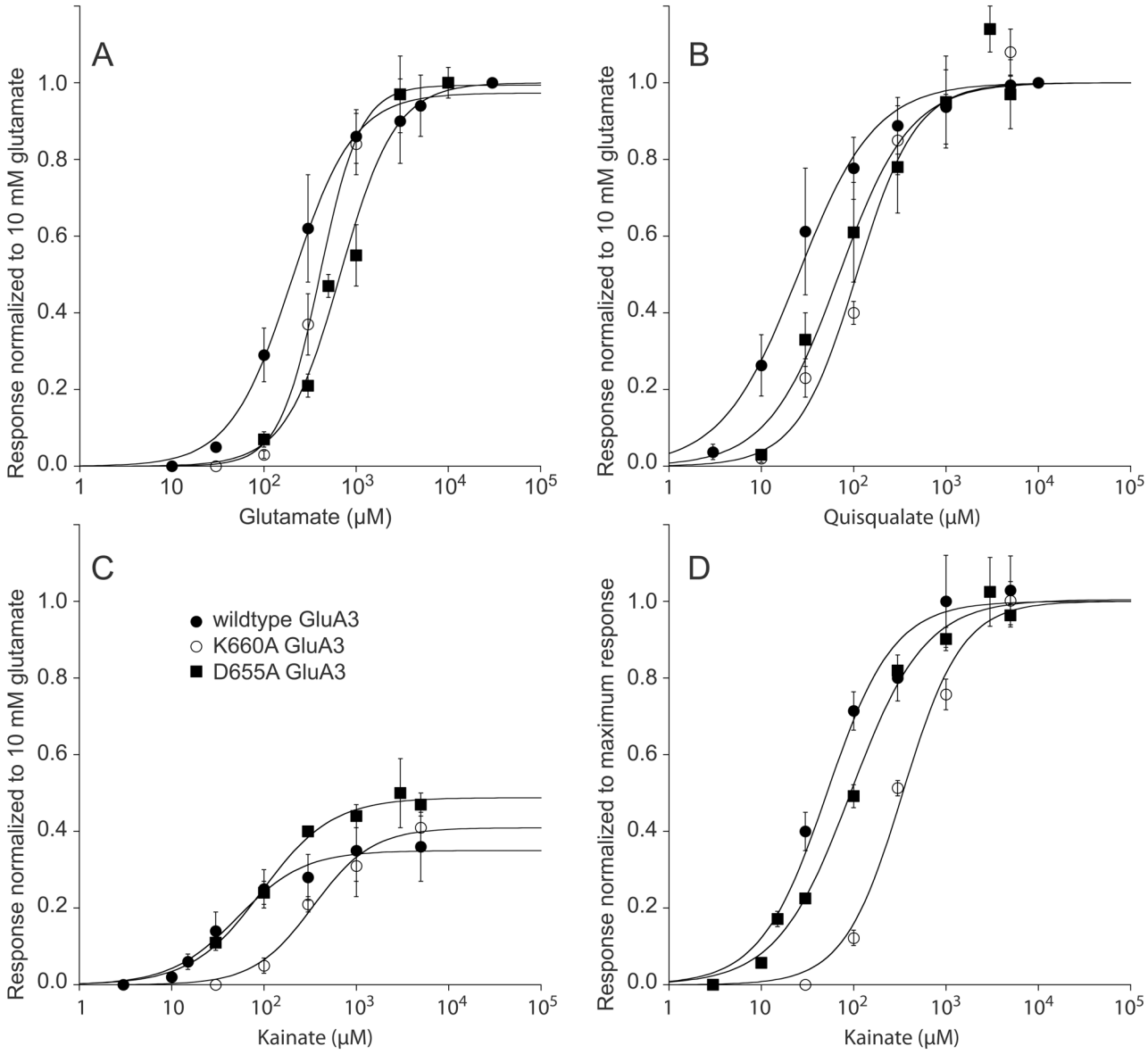

Figure 2. D655A and K660A mutations affect agonist function

A) Glutamate concentration-effect relationships for wildtype GluA3i (filled squares), GluA3i-D655A (open squares) and GluA3i-K660A (open circles). Response curves of mutant receptors are shifted to the right. B) A similar pattern of changes was seen in the quisqualate response curves. C) Kainate was a partial agonist for all three receptors. Kainate efficacy, measured relative to the response to 10 mM glutamate response in the same cells increased significantly ($p < 0.5$) for the D655A mutant compared to wildtype. D) Normalizing the kainate concentration-effect curves to the maximum kainate response obtained (5 mM GluA3i-D655A) illustrates the small rightward shift of the response curve of GluA3i-D655A compared to wildtype GluA3i. Cells (3–15 per agonist concentration) were held at −60 mV and agonist responses (A, B, C) were normalized to the response to 10 mM glutamate (bars: mean ± SD). CTZ (100–150 μM) was present in all recordings. EC_{50} values and Hill slopes are reported in Table 1.

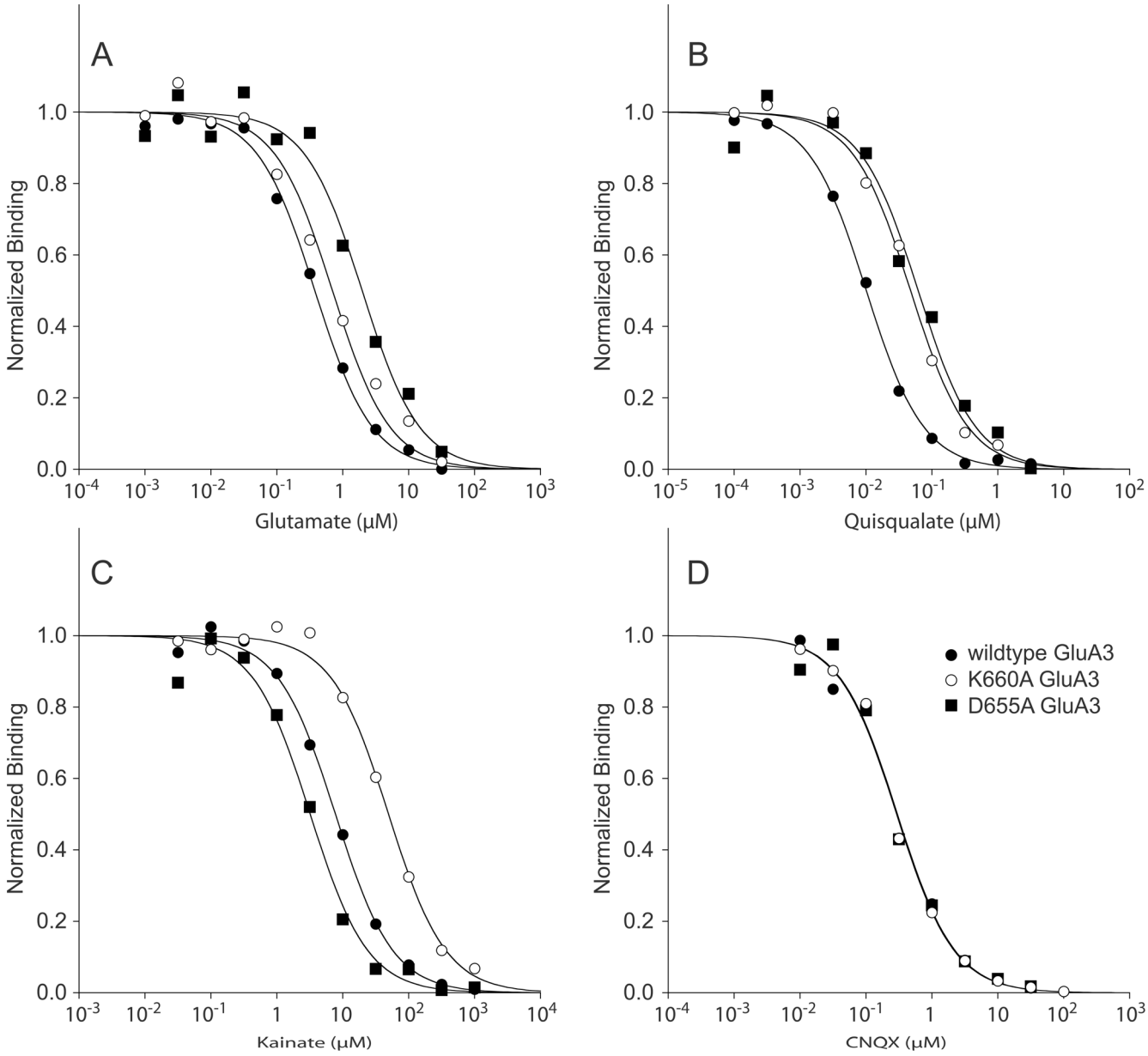

Figure 3. Agonist binding affinity, but not CNQX affinity was affected by D655A and K660A mutations in the GluA3 LBD

Inhibition of the specific binding of the high affinity agonist [^{3}H]AMPA by increasing concentrations of A) glutamate, B) quisqualate, C) kainate, and D) CNQX are shown in wildtype (filled squares), D655A (open squares) and K660A (open circles) LBDs. IC_{50} values for glutamate and quisqualate increased for D655A and K660A compared to wildtype. Kainate's IC_{50} increased in the K660A relative to wildtype and IC_{50} values for CNQX were similar in wildtype, D655A and K660A mutants. AMPA affinity (data not shown) was decreased for the D655A and K660A mutations by ~2-fold. K_i values reported in Table 1 show that kainate affinity was unchanged by the D655A mutation and CNQX binding affinity was the same for all three receptors.

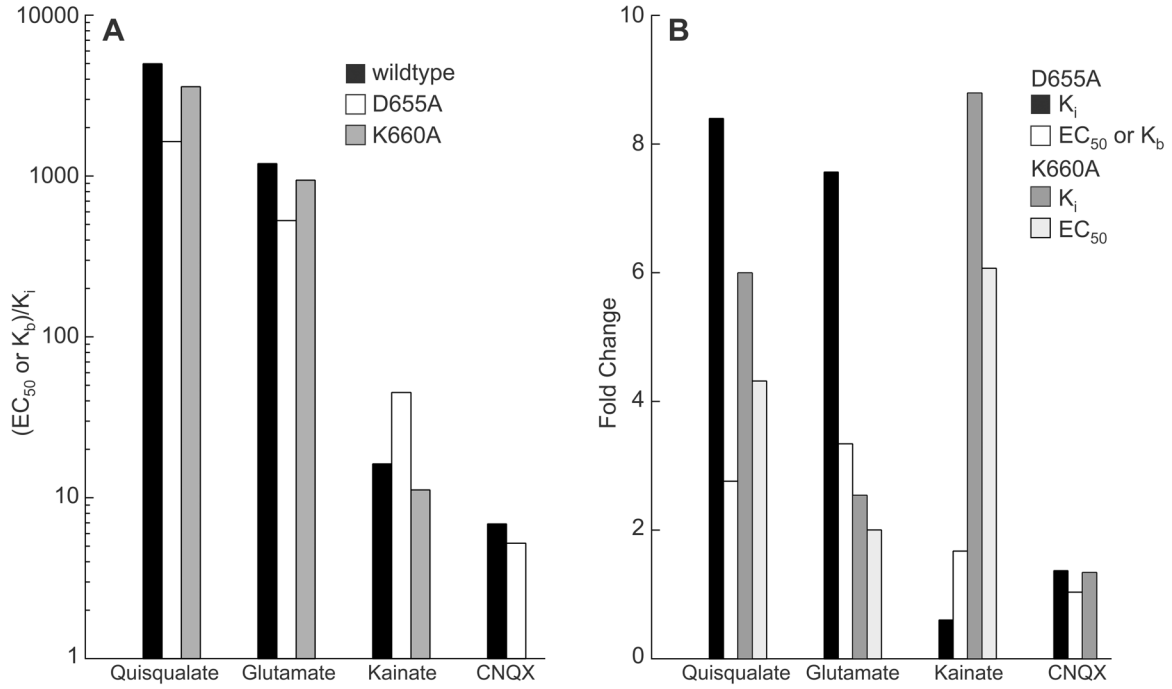

Figure 4. The relationship between ligand potency (EC_{50} or K_b) and ligand binding affinity (Ki) in the mutants is ligand dependent

A) The ratio between the potency of the ligand (EC_{50} or K_b) in the holo receptor to the ligand K_i measured in isolated LBDs reported in Table 1 is plotted for the wildtype, GluA3-D655A and GluA3-K660A receptors. The log difference between functional potency and binding affinity was least for the antagonist CNQX and greatest for the highest affinity agonist quisqualate in wildtype and mutant receptors. B) Bars representing the fold-change in potency and affinity values for mutant receptors compared to wildtype show greater differences for affinity changes than potency changes for full agonists in the D655A mutant than for the partial agonist kainate and the antagonist CNQX. The K660 mutant showed a different agonist-dependent pattern of affinity and potency changes compared to the D655A mutant.

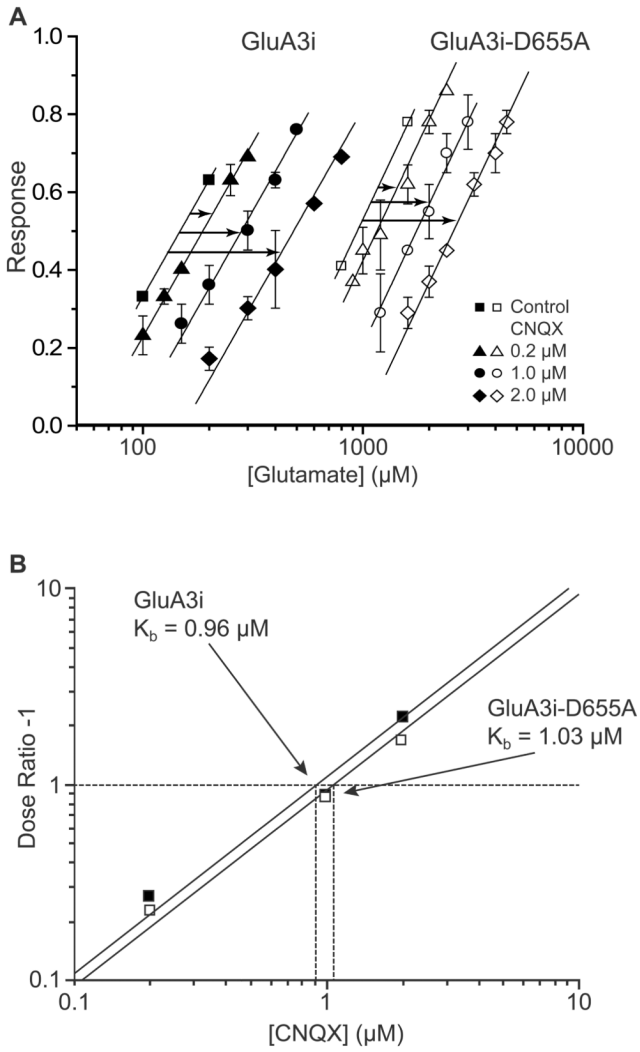

Figure 5. Wildtype and GluA3$_i$-D655A receptor-channels had similar affinity for CNQX

A) Partial glutamate concentration-effect curves were obtained using whole cell currents recorded from cells expressing the wildtype (filled symbols) and the mutant GluA3$_i$ (open symbols), in the absence and presence of the antagonist CNQX. Each data point represents 2–8 cells (mean ± SEM; 2–11 trials per cell). Dose-ratios (DRs) were determined from the rightward shift of the concentration-effect curves (arrows) in increasing concentrations of CNQX. B) Schild plots of log [DR-1] *vs* log [CNQX] for wildtype and GluA3$_i$-D655A data were both fitted by lines with a slope of 1, indicating competitive antagonism. CNQX functional affinity (K_b) was unchanged.

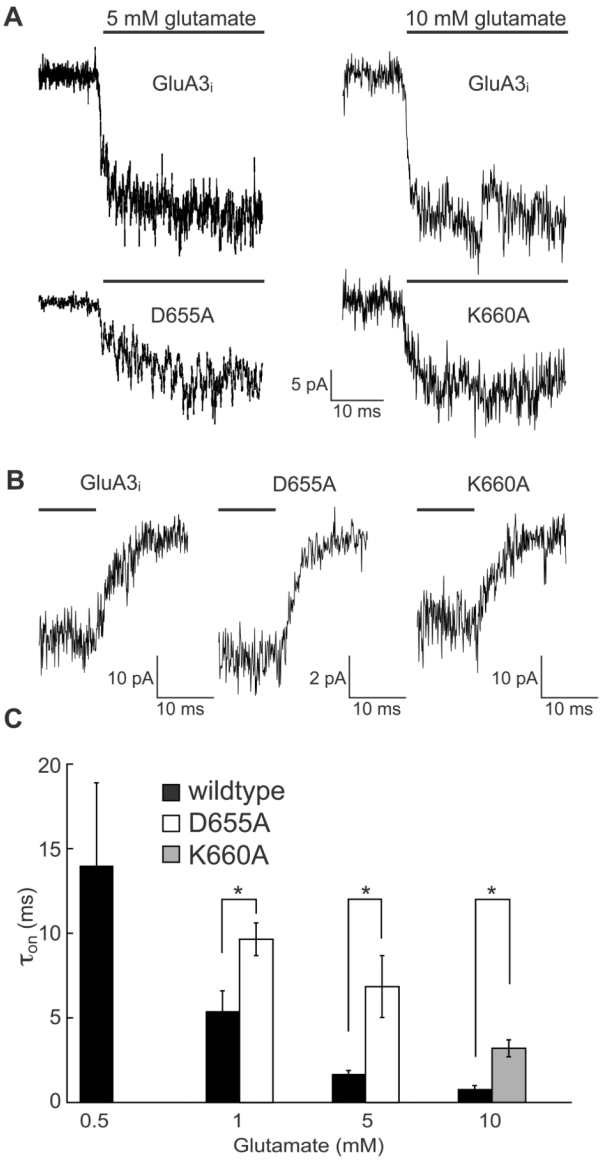

Figure 6. Glutamate response activation is slower in D655A and K660A mutants

A) Traces show responses from outside-out macropatches exposed to rapid application of glutamate (5 mM and 10 mM to patches containing wildtype (top) and the D655A and K660A mutant (bottom) receptor-channels. B) Off-responses of wildtype (left), D655A (center) and K660A (right) receptors obtained after switching to control solution. C) τ_{on} for activation of wildtype (black bars), D655A (white bars) and K660 (gray bar) receptor-channel responses show the influence of increasing glutamate concentration. Wildtype receptors activated faster at all concentrations, including 10 mM glutamate, which produces maximum amplitude responses for wildtype and mutant receptors (see Figure 2). Data were taken from 23 patches held at −100 mV.

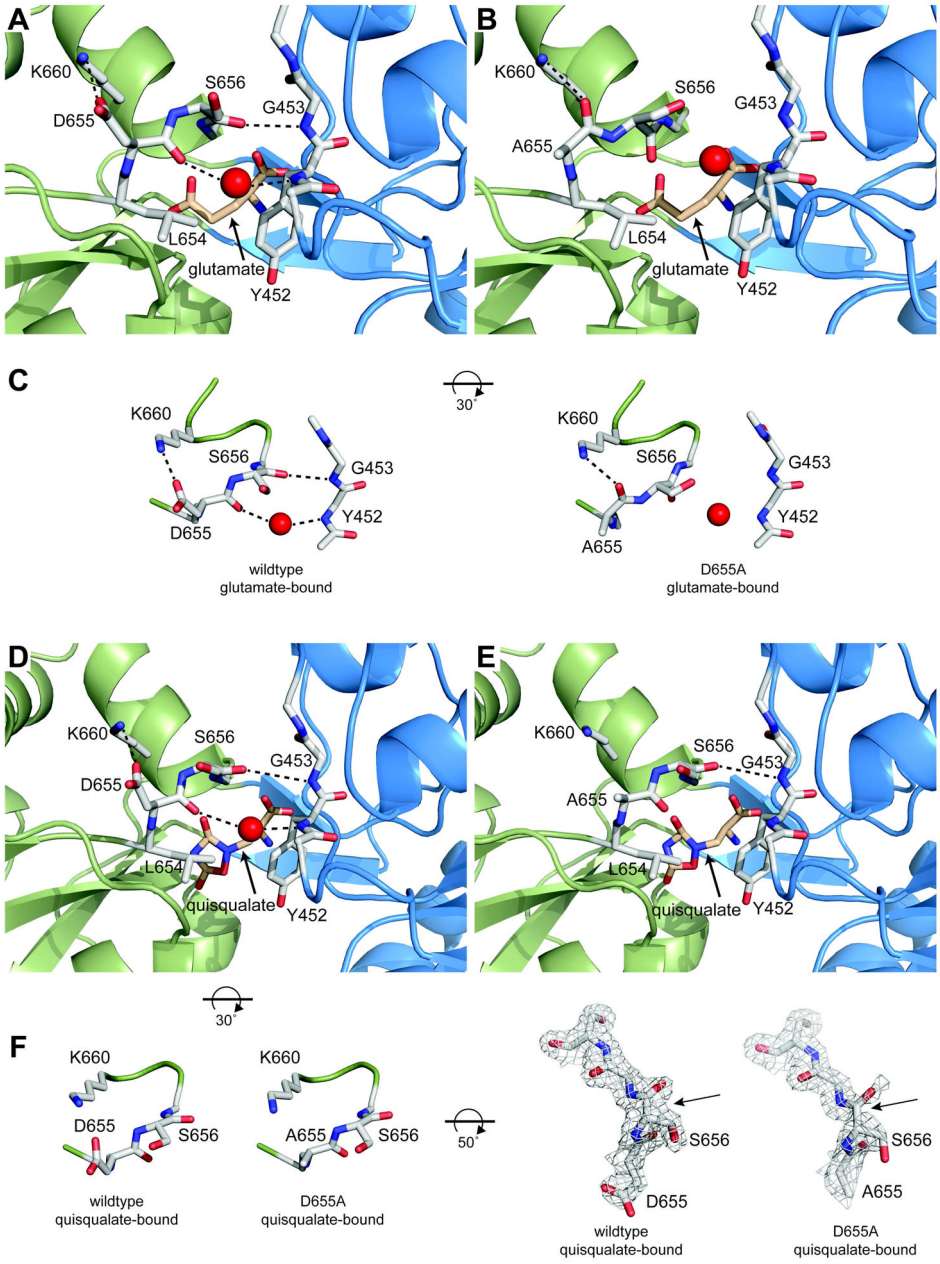

Figure 7. Binding sites for glutamate and quisqualate on the LBD of the wildtype (A, D) and D655A mutant (B, E) receptors

Wildtype GluA3 LBD bound to glutamate (A, C) and quisqualate (D, F) are in the flipped conformation. In the GluA3-D655A mutant, the A655-S656 peptide bond is unflipped in the glutamate-bound form (B, C) and flipped in the quisqualate-bound form (E, F). However, the electron density maps in the quisqualate-bound form are weaker for the S656 backbone in the D655A mutant than in wildtype (arrow in F). The representations in C and the left side of F are rotated 30° round the *x*-axis relative to A, B and D, E, respectively. For the electron density representation on the right side of F, the figure is rotated an additional 50° around the *x*-axis Crystallographic water in the binding site is shown as a red sphere, and the residues involved in the peptide flip region and K660 are shown in a stick representation. Lobe 1 is colored cyan and lobe 2 is green.

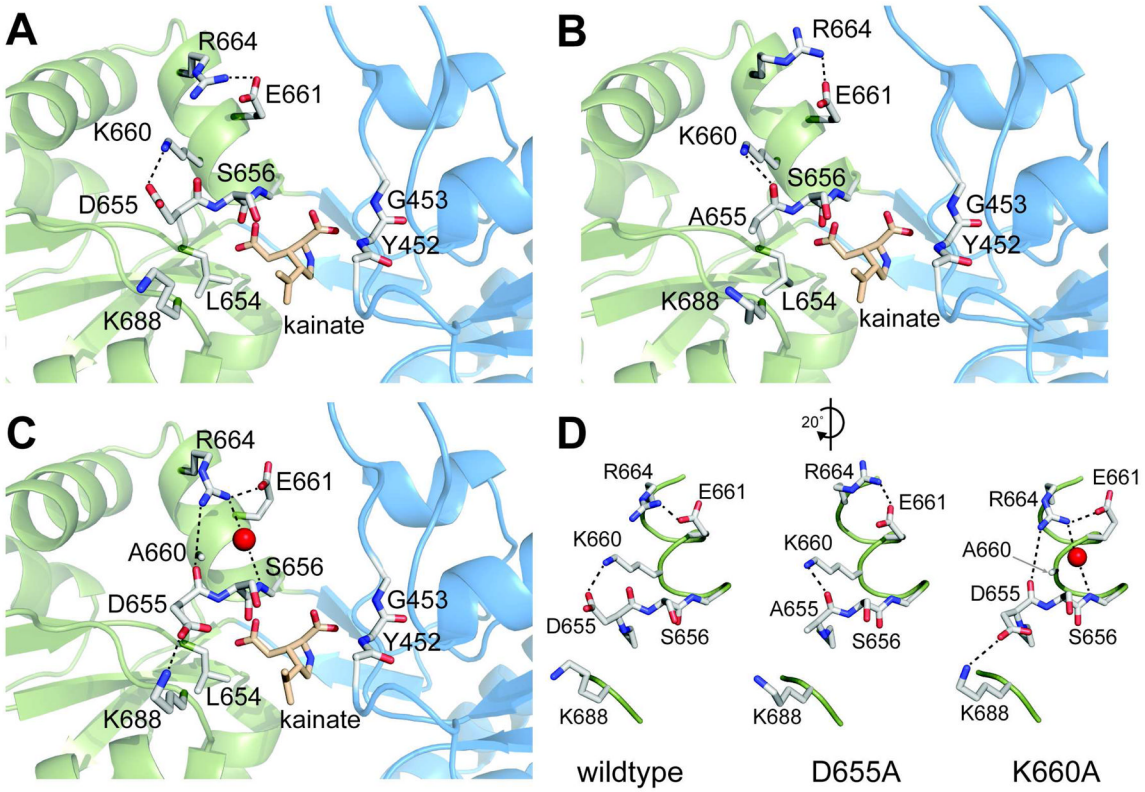

Figure 8. Binding sites for kainate on the LBD of wildtype, D655A and K660A receptors

In all three proteins, the D655/S656 peptide bond was unflipped. (A) In wildtype GluA3 LBD bound to kainate, both the sidechain and backbone carbonyl of D655 can interact with the sidechain in K660. Also, R664 forms a salt bridge with E661. The sidechain of L654 can clash with the isoprenyl group of kainate to keep the lobes partially open, but studies on GluA2 show that it is possible for the sidechain to rotate and the lobes to close fully, although presumably with low probability (*52*). (B) In GluA3-D655A bound to kainate, the interaction between the sidechain of position 655 and K660 is lost, but the carbonyl of A655 now interacts with the sidechain of K660. In this structure, the sidechain of L654 is rotated with respect to wildtype and the lobes are slightly more closed (by 3°). (C) In GluA3-K660A bound to kainate, the electrostatics surrounding the binding site change significantly. A network of interactions involving the side chains of R664 and E661 and the backbone atoms of D655 and S656 replaces the simple salt bridge between R664 and E661. This is apparently due to the additional space and a change in charge as a result of the removal of the sidechain of K660. The sidechain of D655 rotates to interact with K688. L654 is in the same conformation as wildtype and the lobe closure is similar to wildtype. The red sphere is a crystallographic water molecule. Lobe 1 is colored cyan and lobe 2 is green. (D) Changes in the electrostatic interactions from wildtype to the D655A and K660A mutants are illustrated. The figures are rotated 20° around the *y*-axis relative to (A,B,C).

Table 1

Pharmacologic parameters of wildtype and mutant *holo* receptors and LBDs

Ligand: receptor	**EC_{50} (μM)**	**** Efficacy**	**Hill#**	*****IC_{50}(μM)**	**K_i (μM)**	**EC_{50}/K_i**
AMPA						
wildtype	ND	–	–	0.006	*0.009*$^{\wedge}$	–
D655A	ND	–	–	0.024	0.020	–
K660A	ND	–	–	0.029	0.0173	–
Quisqualate						
wildtype	25±7	1	1.0	0.010±0.000	*0.005*$^{\wedge *}$	5000
D655A	69±14	1	1.1	0.062±0.008	0.042	1643
K660A	108±9	1	1.4	0.047±0.004	0.030	3600
Glutamate						
wildtype	201±55	1	1.3	0.379±0.022	*0.168*$^{\wedge *}$	1196
D655A	672±73	1	1.5	1.970±0.287	1.271	529
K660A	403±14	1	2.0	0.699±0.090	0.427	944
Kainate						
wildtype	56±18	0.35	1.2	7.75±0.44	*3.44*$^{\wedge *}$	16
D655A	94±9	0.48	1.1	3.22±0.40	2.08	45
K660A	340±50	0.41	1.4	49.5±4.10	30.26	11
CNQX	$^{*}K_b$					K_b/K_i
wildtype	0.96	–	–	0.295	*0.139*$^{\wedge *}$	7
D655A	1.00	–	–	0.301±0.033	0.191	5
K660A	ND	–	–	0.294±0.028	0.187	–

$^{*}K_b$ from Schild analysis,

**Relative to glutamate,

***ligand binding,

$^{\wedge}K_d$ from AMPA direct binding was used to calculate

[^1]: * K_i of other ligands in the wildtype GluA3 LBD. Errors are ± SEM.